Journal of Power Sources 270 (2014) 326–331

Contents lists available at ScienceDirect

Journal of Power Sources

journal homepage: www.elsevier.com/locate/jpowsour

Preparation of novel network nanostructured sulfur composite cathode with enhanced stable cycle performance

Yongguang Zhang [a], Yan Zhao [a], Zhumabay Bakenov [c], Aishuak Konarov [b], P. Chen [b, *]

[a] Research Institute for Energy Equipment Materials, Hebei University of Technology, 8 Guangrong Road, Tianjin 300130, China
[b] Department of Chemical Engineering, University of Waterloo, 200 University Avenue West, Waterloo, ON N2L3G1, Canada
[c] Institute of Batteries LLC, Nazarbayev University, 53 Kabanbay Batyr Avenue, Astana 010000, Kazakhstan

HIGHLIGHTS

- S/PAN composite was prepared via *in situ* polymerization of acrylonitrile.
- S/PAN composite with network-like structure was used as cathode in a Li/S battery.
- The resulting S/PAN composite showed enhanced cyclability and rate capability.

ARTICLE INFO

Article history:
Received 24 April 2014
Received in revised form
15 July 2014
Accepted 15 July 2014
Available online 22 July 2014

Keywords:
Lithium/sulfur battery
Sulfur/polyacrylonitrile composite
Network structure
Cathode

ABSTRACT

In situ polymerization of acrylonitrile with nano-sulfur particles has been developed as a synthetic route to prepare sulfur/polyacrylonitrile (S/$_p$PAN) composite as a cathode material for lithium/sulfur battery. Transmission electronic microscopy revealed the formation of a highly developed network structure consisting of PAN and sulfur homogeneous mixing at nanosized level, providing the "buffering" space to accommodate the volume change of sulfur upon cycling and retaining the structural integrity preventing the material agglomeration and degradation. Benefiting from this unique structure, the S/$_p$PAN composite cathode demonstrated enhanced reversibility, resulting in a discharge capacity of 1177 mAh g^{-1} at the second cycle and retained about 100% of this value over 100 cycles at 0.5C. Furthermore, the S/$_p$PAN composite cathode delivered a discharge capacity of 981 mAh g^{-1} at the 100th cycle at 1C.

1. Introduction

Lithium/sulfur (Li/S) batteries have been considered one of the most attractive power sources for hybrid electric and electric vehicles, and large scale energy storage systems due to a high theoretical capacity of 1672 mAh g^{-1} achievable with the sulfur cathode [1]. Along with this, sulfur is inexpensive, high abundance and nontoxic. However, despite of these great promises, there are still a number of problems hindering the application of Li/S batteries [2,3]. First of all, sulfur could be considered an electric insulator, which leads to poor electrochemical accessibility and a low electrochemical utilization of sulfur in the electrode. Another major problem is related with high solubility of lithium polysulfides as intermediate products generated during discharge/charge process, leading to a rapid active mass loss of the cathode, the shuttle effect and side reactions of these products on the lithium anode surface causing a serious capacity fading upon cycling. Furthermore, the volume expansion of this cathode material is as high as 80%, when sulfur is fully converted to Li_2S. This volume change causes the pulverization of active materials and thus fast capacity fading [4,5].

Great efforts have been devoted to overcome these problems and improve the Li/S system performance; various types of conductive carbon materials and conductive polymers have been used in order to enhance the electric conductivity of the composite and hinder the dissolution of the polysulfides into the electrolyte [6–17].

From this point of view, the fabrication of sulfur/polyacrylonitrile (S/PAN) composites has been proven to be promising, and S/PAN composites have demonstrated high sulfur utilization along with a high initial capacity [8]. Nevertheless, the high particle agglomeration of the S/PAN composite upon cycling and a consequent inter-particle contact loss hinder the cyclability and rate capability of this composite, and it is still challenging to disperse sulfur homogeneously in the S/PAN composite [9]. Therefore, the

* Corresponding author. Tel.: +1 519 888 4567x35586; fax: +1 519 746 4979.
E-mail address: p4chen@uwaterloo.ca (P. Chen).

http://dx.doi.org/10.1016/j.jpowsour.2014.07.096
0378-7753/

development of a novel technique to prepare the S/PAN composite with homogeneous sulfur distribution in the polymer matrix is crucial to enhance this cathode performance.

Herein, we developed a nanostructured S/PAN composite with an original network-like structure via *in situ* polymerization of acrylonitrile (AN) in the presence of nanosized S particles followed by a low temperature heat treatment, and herein, its physical and electrochemical properties as a cathode for lithium secondary batteries were investigated.

2. Experimental

Nanosized PAN was synthesized by dispersion/emulsion polymerization process [18]. 0.62 mL acrylonitrile (AN) (ACROS, 99% purify), 10 mg potassium persulfate (PPS) (EMD, 99% purify), and 0.1 g sodium dodecyl sulfate (SDS) (Sigma–Aldrich, ≥99% purify) were dissolved in 9.38 mL deionized water followed by thorough stirring at 70 °C for 10 h. The resulting system was washed by intensive centrifugation cycles with deionized water and then vacuum dried overnight at 70 °C.

The original composite cathode, denoted further as S/$_p$PAN, was synthesized by *in situ* polymerization of AN along with sulfur nanoparticles. 0.62 mL AN, 10 mg PPS, and 0.1 g SDS was added into 20 g aqueous suspension of nano-sulfur (US research nanomaterials Inc, 10 wt%) and thoroughly stirred at 70 °C for 10 h. The resulting precursor mixture was washed by intensive centrifugation cycles with water and then vacuum dried overnight at 70 °C, and then was heat treated at 350 °C for 6 h in a tubular furnace in Ar gas to melt sulfur and react it with PAN.

For comparison purposes, the composite cathode, denoted further as S/$_c$PAN, was prepared by mixing of sulfur (Sigma–Aldrich, 100-mesh particle size powder) and polyacrylonitrile (PAN) (Sigma–Aldrich) in the weight ratio of 4:1 by ball milling (Fritsch, Pulverisette 7 Classic Line) at 600 rpm for 3 h with *n*-methyl-2-pyrrolidinone (NMP, Sigma–Aldrich) as a dispersant. The mixture (precursor) was further dried in a vacuum oven at 70 °C for 12 h to remove the solvent and then heat treated at 350 °C for 6 h in a tubular furnace in Ar gas to melt sulfur and react it with PAN.

Structure of the composites was characterized using the Fourier transform infrared spectroscopy (FT-IR, 520, Nicolet). The crystalline phases of the samples were determined by X-ray diffraction (XRD, D8 Discover, Bruker) analysis equipped with Cu-Kα radiation. The interior structure of the composite was observed by using transmission electron microscopy (TEM, CM10, Philips) at 60 kV. The composite surface morphology was examined by scanning electron microscopy (SEM, JSM-6490, JEOL) with energy dispersive spectroscopy (EDS) mapping. The sulfur content of S/PAN composite was analyzed using an element analyzer (CHNS, Vario Micro Cube, Elementar). Chemical analysis has shown that the sulfur content in the S/$_p$PAN and S/$_c$PAN composite were 40.9 wt% and 43.2 wt%, respectively.

CR2032 coin-type cells were assembled inside a MBRAUN glove box filled with high purity argon (99.9995% Ar) by sandwiching a polypropylene separator (Celgard, USA) between the composite cathode and lithium anode, and using 1 mol dm^{-3} lithium hexafluorophosphate ($LiPF_6$) in ethylene carbonate:dimethylcarbonate:diethyl carbonate (EC:DMC:DEC) = 1:1:1 as electrolyte (EMD chemicals Inc., Selectlyte Battery Electrolyte LP40). The cathode was comprised of 80 wt% binary composite, 10 wt% acetylene black (AB, MTI Co.) as a conductive agent and 10 wt% polyvinylidene fluoride (PVdF, Kynar, HSV900) as a binder. These materials were dispersed in NMP. The resultant slurry was spread onto an Al foil (MTI, ≥99% purity), dried in vacuum oven for 12 h at 60 °C and then cut into the circles of 1 cm in diameter. The electrodes were prepared to make their weight and thickness the same by precise weighing, pressing and controlling their geometry. The active material (S/PAN composite) loading in each electrode was about 2 mg cm^{-2}, and the thickness of the electrode film was about 80 μm. The cells were tested galvanostatically on multichannel battery tester (BT-2000, Arbin) between 1 and 3 V *vs.* Li^+/Li at various current densities. Applied currents and specific capacities were calculated on the basis of the weight of S in the composite cathode. Cyclic voltammetry (CV) was performed with a potentiostat/galvanostat (VMP3, BioLogic) between 1 and 3 V *vs.* Li^+/Li at a scanning rate of 0.1 mV s^{-1}. The electrochemical impedance spectroscopy (EIS) measurements were carried out using a potentiostat/galvanostat VMP3 by applying an ac voltage of 10 mV over the frequency range of 0.1 Hz–1 MHz. All electrochemical measurements were performed at room temperature.

3. Results and discussion

The similarity in the molecular structure of as-prepared PAN ($_p$PAN) and commercial PAN ($_c$PAN) samples has been confirmed from the FT-IR analysis as shown in Fig. 1. Characteristic peaks at 2244 cm^{-1} representing the –CN groups and those at 1455 cm^{-1} related to the $-CH_2$ group peaks can be seen in the spectra of both samples [18]. This indicates that PAN was successfully obtained via the chemical polymerization method during the $_p$PAN synthesis. The XRD patterns (Fig. 2) offer additional information about the structure evolution in the polymerization of AN in the presence of S. It can be seen that obvious typical reflection of PAN at 16.8° is present in both $_p$PAN and $_c$PAN, which confirms the FT-IR results above, and the $_p$PAN and $_c$PAN samples have similar chemical composition and crystal structure. One can see that the characteristic *Fddd* orthorhombic crystal structure peaks of elemental sulfur disappear from the XRD patterns of the S/$_p$PAN composite. This could be an indication that sulfur exists in the composite as embedded fine particles distributed in the pyrolyzed PAN matrix. The TEM images of $_c$PAN and $_p$PAN are shown in Fig. 3a and b. The $_c$PAN composite particles (Fig. 3a) are highly agglomerated. In contrast, as shown in Fig. 3b, the PAN particles prepared via *in situ* polymerization of AN have spherical shape and are well dispersed. The inset of Fig. 3b presents the PAN particle diameter distribution obtained from the analysis of the TEM data. $_p$PAN particles have uniform diameter distribution with a geometric mean diameter of $d_{g,p} = 125$ nm and a geometric standard deviation of $\sigma_g = 1.18$. The comparative data of the TEM results for the S/$_c$PAN and S/$_p$PAN composites could be observed in Fig. 3c and d. In contrast to the severely agglomerated S/$_c$PAN composite particles, the S/$_p$PAN composite shows a well-dispersed network-like structure; it forms a nanostructured system, where

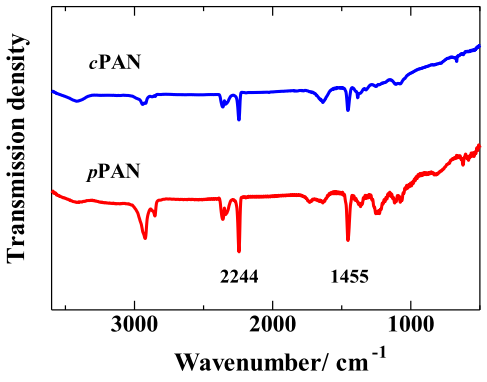

Fig. 1. FTIR spectra of $_c$PAN and $_p$PAN samples.

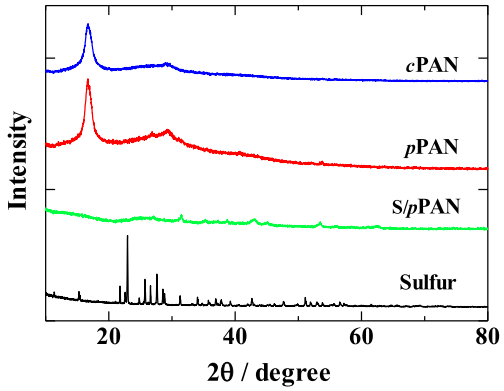

Fig. 2. XRD patterns of $_c$PAN, $_p$PAN, S/$_p$PAN composite and sulfur precursor.

the particles are connected with each other via a highly developed network structure.

Results of EDS mapping for C and S in S/$_p$PAN are shown in the inset of Fig. 4a. The bright regions represent these elements distribution in the composite, and indicate that S and C are distributed uniformly within the samples. Fig. 4 shows the SEM images of fresh and cycled S/$_c$PAN and S/$_p$PAN composite cathodes. It can be seen from Fig. 4a and b that the morphology of the S/$_p$PAN composite does not change remarkably after cycling. This morphology stability could be due to the network nanostructure of S/$_p$PAN composite, which could provide the "buffering" space to accommodate the volume changes of sulfur upon cycling, retaining its structural integrity and preventing material agglomeration and degradation. In contrast, the S/$_c$PAN composite cathode morphology (Fig. 4c and d) changes drastically upon cycling, and the active material particles in this composite continuously merge into large agglomerates, negatively affecting the cathode conductivity and sulfur utilization. This agglomeration leading to reduced conductivity of the S/$_c$PAN composite could be one of the major reasons of its poor cyclability.

Fig. 5 presents the 1st, the 5th and the 10th CV cycles of the S/$_p$PAN composite. One can see that at the initial cycle there is a pronounced reduction process, which could be due to the side reactions of formation of a solid electrolyte interface (SEI), and these processes lead to a larger polarization between the reduction and oxidation peaks. It could also be suggested that these processes are inherent only for the first cycle because they are not present in the following CV cycles. After the initial activation, on the following cycles the S/$_p$PAN composite exhibits two major stages of the redox processes in the system, which agrees with the literature data and could be attributed to the transition of S to high-order lithium polysulfides (Li_2S_n, $n \geq 4$), and their further transition into lithium sulfide (Li_2S), respectively [10,13]. Meanwhile, after the initial cycle, the current of the peaks keeps unchanged upon the subsequent cycles, which confirms a good reversibility of the studied system. The S/$_p$PAN composite cathode performance was remarkably enhanced compared with that of the S/$_c$PAN cathode as shown in Fig. 6a and b. Upon the galvanostatic cycling at 0.5C (0.7 mA cm^{-2}),

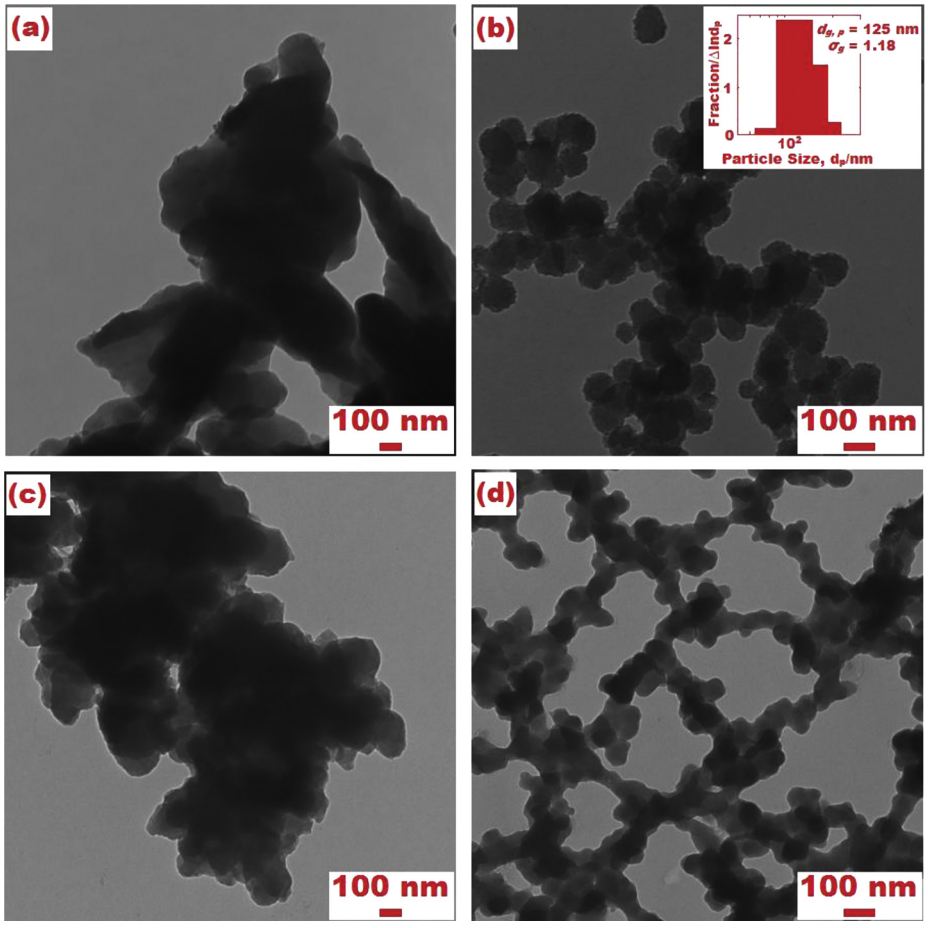

Fig. 3. TEM images of (a) $_c$PAN, (b) $_p$PAN, (c) S/$_c$PAN composite and (d) S/$_p$PAN composite samples.

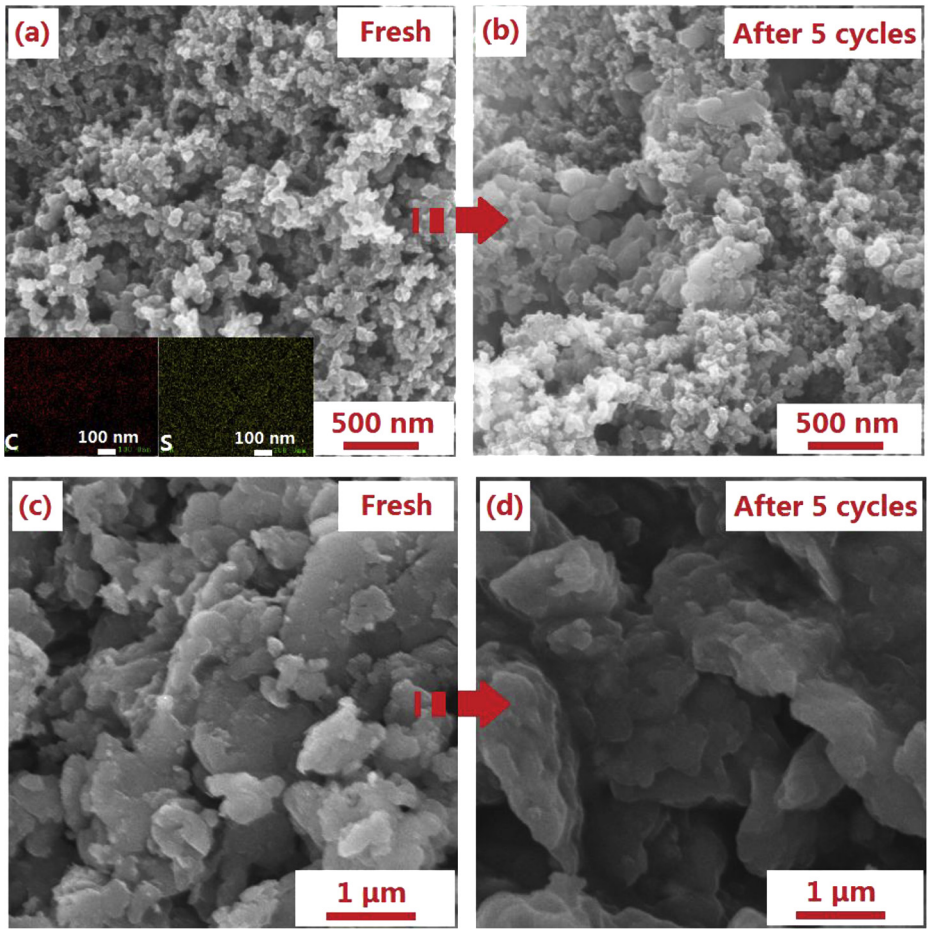

Fig. 4. SEM images of (a, b) S/$_p$PAN composite and (c, d) S/$_c$PAN composites before and after discharge–charge cycles; Inset of (a): EDS mapping showing the distribution of C and S elements.

a cell with the S/$_p$PAN composite cathode delivered a specific capacity of 1510 mAh g^{-1} at the first cycle, and a very high reversible capacity of 1177 mAh g^{-1} was achieved at the following cycle. The cell exhibited the excellent cyclability retaining about 100% of its initial reversible discharge capacity after 100 cycles at 0.5C. Although both cathodes exhibit a high coulombic efficiency (about 100%) over 100 cycles, which could be attributed to the shuttle effect suppression in the S/PAN composite, the S/$_c$PAN composite electrode suffers from a rapid capacity fading and loses about 53%

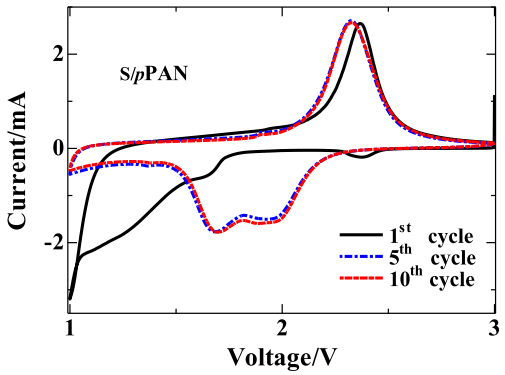

Fig. 5. CV profiles of lithium cells with the S/$_p$PAN composite cathode (scan rate is 0.1 mV s^{-1}).

of its initial capacity after 100 cycles of discharge/charge. The performance improvement of S/$_p$PAN composite cathode compared with the S/$_c$PAN counterpart could be attributed to the multiple effects of the networking structure such as buffering ability to absorb the mechanical stress induced by the volume changes of sulfur cathode upon cycling, the ability to retain the structural integrity of the composite preventing the material agglomeration and degradation. The kinetic behavior of the S/$_p$PAN composite was further evaluated via cycling the cell with this cathode at the higher current density. The cyclability results for these conditions are shown in Fig. 7. It can be seen that the initial capacity of 1265 mAh g^{-1} was achieved at 1C (1.4 mA cm^{-2}), and after 100 cycles the cell retains a capacity of 981 mAh g^{-1}, demonstrating an enhanced rate capability of the S/$_p$PAN composite prepared in this work. This performance improvement are attributed to the nano-sized network-structure of the S/$_p$PAN composite, which could provide the very short diffusion paths for the charge carriers and favors in the deeper good penetration of the electrolyte into the electrode volume. A cooperative effect of these advantages in the physico-chemical properties favors the remarkable electrochemical kinetic improvements.

The composite cathode conductivity enhancement could be confirmed by comparison of EIS data of the cells with S/$_c$PAN and S/$_p$PAN composite cathodes (the fresh cells) presented in Fig. 8. Both cathodes exhibited the Nyquist plots comprising of a compressed semicircle in the high to medium frequency range,

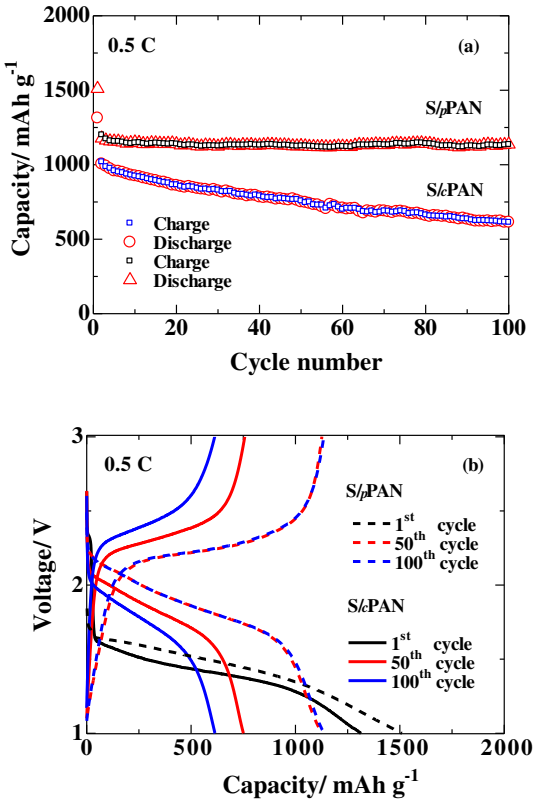

Fig. 6. (a) Comparative data on cyclability of lithium cells with the S/$_c$PAN and S/$_p$PAN composite cathodes at 0.5C; (b) discharge/charge profiles of lithium cells with the S/$_c$PAN and S/$_p$PAN composite cathodes at 0.5C.

attributed to the charge transfer impedance [19] and an inclined line in the lower frequency range, which could be represented by a Randles equivalent circuit [20]. The inclined line in the lower frequency represented the Warburg impedance, associated with lithium-ion diffusion in the electrode particles. It can be seen that the high-to-medium frequency semicircle was observed in the S/$_p$PAN electrode EIS spectra has much smaller in diameter compared with that of the S/$_c$PAN cathode, which indicates a significantly lower charge transfer resistance of the S/$_p$PAN composite compared with the S/$_c$PAN counterpart. We attribute the charge transfer enhancement to the nanosized network-structure of the S/$_p$PAN composite, offering the shorter diffusion paths for the charge carriers and favoring in the deeper and enhanced penetration of the electrolyte into the electrode volume.

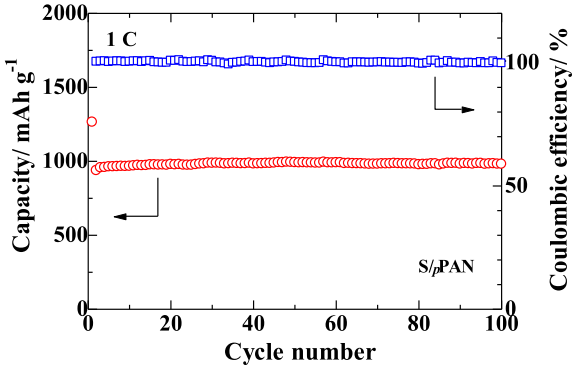

Fig. 7. Cycling performance of lithium cells with the S/$_p$PAN composite cathodes at 1C.

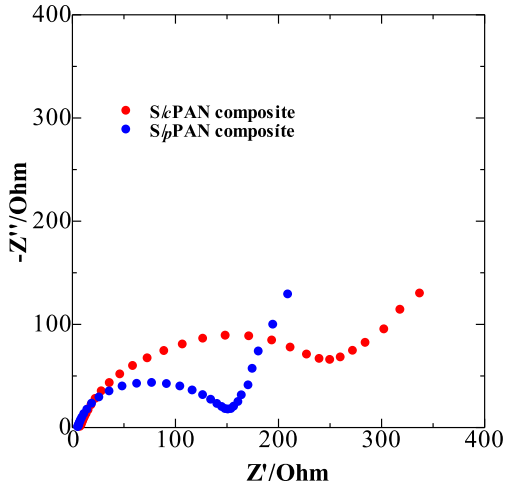

Fig. 8. EIS analysis of the S/$_c$PAN and S/$_p$PAN composites.

4. Conclusions

A nanostructured sulfur/polyacrylonitrile (S/$_p$PAN) composite with a network structure was prepared via *in situ* polymerization of acrylonitrile in the presence of nanosized sulfur particles followed by a heat treatment. The composite has well dispersed network structure with the interconnected particles. This structure preserves the system from the agglomeration and degradation, buffering the mechanical stresses upon cycling. Furthermore, the interconnected (network) nanosized structure reduces the length of the Li-ion diffusion paths, favoring remarkable electrochemical kinetic improvements. The S/$_p$PAN composite exhibits very attractive performance of a promising cathode material for high energy density Li/S batteries.

Acknowledgments

This research was financially supported by Positec, Natural Sciences and Engineering Research Council of Canada (NSERC), Canadian Foundation for Innovation (CFI) and the Canada Research Chairs (CRC). YZ thanks the China Scholarship Council for Study Abroad Scholarship. ZB acknowledges a research grant from the Ministry of Education and Science of Kazakhstan #1889 and a Subproject supported by the Technology Commercialization Project by the World Bank and the Government of Kazakhstan.

References

[1] A. Manthiram, Y. Fu, Y.S. Su, Acc. Chem. Res. 46 (2013) 1125–1134.
[2] Y. Zhao, Y. Zhang, D. Gosselink, T.N.L. Doan, M. Sadhu, H. Cheang, P. Chen, Membranes 2 (2012) 553–564.
[3] Y. Zhang, Y. Zhao, K.E.K. Sun, P. Chen, Open Mater. Sci. J. 5 (2011) 215–221.
[4] M.K. Song, E.J. Cairns, Y. Zhang, Nanoscale 5 (2013) 2186–2204.
[5] Y. Yang, G. Zheng, Y. Cui, Chem. Soc. Rev. 42 (2013) 3018–3032.
[6] Y. Zhang, Z. Bakenov, Y. Zhao, A. Konarov, T.N.L. Doan, K.E.K. Sun, A. Yermukhambetova, P. Chen, Powder Technol. 235 (2013) 248–255.
[7] Y. Zhao, Y. Zhang, Z. Bakenov, P. Chen, Solid State Ionics 234 (2013) 40–45.
[8] Y. Zhang, Y. Zhao, A. Yermukhambetova, Z. Bakenov, P. Chen, J. Mater. Chem. A 1 (2013) 295–301.
[9] K. Jeddi, Y. Zhao, Y. Zhang, A. Konarov, P. Chen, J. Electrochem. Soc. 160 (2013) A1052–A1060.
[10] Y. Zhang, Z. Bakenov, Y. Zhao, A. Konarov, T.N.L. Doan, M. Malik, T. Paron, P. Chen, J. Power Sources 208 (2012) 1–8.
[11] W. Wang, G.C. Li, Q. Wang, G.R. Li, S.H. Ye, X.P. Gao, J. Electrochem. Soc. 160 (2013) A805–A810.
[12] Y. Zhang, Y. Zhao, A. Konarov, D. Gosselink, Z. Li, M. Ghaznavi, P. Chen, J. Nanopart. Res. 15 (2013) 2007.

[13] Y. Zhang, Y. Zhao, A. Konarov, D. Gosselink, H.G. Soboleski, P. Chen, Solid State Ionics 238 (2013) 30–35.
[14] C. Wang, W. Wan, J.T. Chen, H.H. Zhou, X.X. Zhang, L.X. Yuan, Y.H. Huang, J. Mater. Chem. A 1 (2013) 1716–1723.
[15] Y. Zhang, Y. Zhao, A. Konarov, D. Gosselink, H.G. Soboleski, P. Chen, J. Power Sources 241 (2013) 517–521.
[16] B. Ding, C. Yuan, L. Shen, G. Xu, P. Nie, X. Zhang, Chem. Eur. J. 19 (2013) 1013–1019.
[17] Y. Zhang, Y. Zhao, Z. Bakenov, M.R. Babaa, A. Konarov, C. Ding, P. Chen, J. Electrochem. Soc. 160 (2013) A1194–A1198.
[18] L. Boguslavsky, S. Baruch, S. Margel, J. Colloid Interface Sci. 289 (2005) 71–85.
[19] S.K. Martha, B. Markovsky, J. Grinblat, Y. Gofer, O. Haik, E. Zinigrad, D. Aurbach, T. Drezen, D. Wang, G. Deghenghi, I. Exnar, J. Electrochem. Soc. 156 (2009) A541–A552.
[20] Z. Bakenov, I. Taniguchi, J. Power Sources 195 (2010) 7445–7451.